Available online at www.sciencedirect.com

ScienceDirect

journal homepage: www.elsevier.com/locate/he

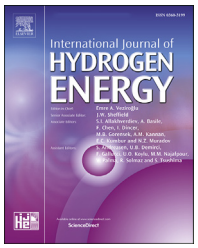

A facile and economical approach to fabricate a single-piece bipolar plate for PEM electrolyzers

Holger Janßen [a,*], *Sebastian Holtwerth* [a], *Walter Zwaygardt* [a], *Andrea Stähler* [a], *Wilfried Behr* [b], *Dirk Federmann* [b], *Marcelo Carmo* [c,1], *Werner Lehnert* [a,d], *Martin Müller* [a]

[a] *Forschungszentrum Jülich GmbH, Institute of Energy and Climate Research, IEK-14: Electrochemical Process Engineering, 52425, Jülich, Germany*

[b] *Forschungszentrum Jülich GmbH, Central Institute of Engineering, Electronics and Analytics, ZEA-1: Engineering and Technology, 52425, Jülich, Germany*

[c] *Mechanical and Materials Engineering, Queen's University, Kingston, ON, K7L 3N6, Canada*

[d] *RWTH Aachen University, Modeling in Electrochemical Process Engineering, 52056, Aachen, Germany*

HIGHLIGHTS

- Detailed insight into the plate design, construction, production and verification.
- Main feature of the novel bipolar plate is the one-piece-approach.
- Development of a welding-based production process; elimination of contact resistances.
- Approach increases the reliability and decreases the duration of the stack assembly.

ARTICLE INFO

Article history:
Received 7 June 2023
Received in revised form
8 September 2023
Accepted 17 September 2023
Available online 11 October 2023

Keywords:
PEM water electrolyzers
Cross-flow configuration
Expanded mesh sandwich
One-piece bipolar plate
Diffusion welding

ABSTRACT

Water electrolysis will be an essential element of the future energy system, with hydrogen serving as a climate-friendly energy storage medium. To make electrolyzers suitable for market penetration at scale, the cost of manufacturing megawatt electrolyzers must be minimized, with no detrimental effects to their performance and lifetime. Here we show a facile and cost-effective manufacturing method to produce one-piece Ti-based bipolar plates. Low-cost and commercially and readily available feedstock materials (blank sheets, expanded metals and nonwovens) are positively joined using an innovative welding process, diffusion bonding. This approach reduces the contact resistances that can occur with multi-part bipolar plates by around 75%, reducing the number of components and therefore significantly simplifying stack assembly. Ex-situ tests on the contact pressure distribution on the active cell surface reveal a homogeneous pattern with values of about 3.75 MPa (± 1.25 MPa). In a first proof-of-concept, a five-cell short stack with a 100 cm^2 active cell area, average cell voltages of 1.71 V at 2 A cm^{-2} could be achieved using our new stack concept.

* *Corresponding author.*
E-mail address: h.janssen@fz-juelich.de (H. Janßen).
[1] Present affiliation: NEL Hydrogen, Wallingford, Connecticut 06492, USA; email: mcarmo@nelhydrogen.com.

https://doi.org/10.1016/j.ijhydene.2023.09.175

1. Introduction

Future energy supply scenarios [1–3] foresee a significant share of renewables, such as wind, solar and hydropower. Due to large and frequent fluctuations in energy supply and demand, an energy storage solution of equal magnitude and of high level of sustainability is required, and hydrogen is indeed considered to be the only viable solution to reach such goals. The associated technology for hydrogen production, namely water electrolysis, already has a high technology readiness level TRL of 6–9 [4]. The TRL for alkaline electrolysis is higher than for Polymer Electrolyte Membrane (PEM) electrolysis. Systems in several power classes are already commercially-available, but still not available in the mass market.

The flexible electrolysis also has a high potential for commercialization, because it can easily serve as a controllable load on the electricity balancing market [5]. In a study at the "Energiepark Mainz", typical operation of an electrolyzer for an energy system participating in the energy market was demonstrated. In addition, it showed the requirements necessary for the pressure operation of an electrolyzer [6]. In order to be able to guarantee energy storage, electrolyzer systems in the high MW, up to the GW scale, will be needed in the future. To meet high-power demand, electrolysis stacks in the MW class and above will be required.

The operating pressure is an important factor influencing the efficiency of an electrolyzer system [7]. Hydrogen is currently stored at high pressures (up to 700 bar for automotive applications) in gas storage systems. Thus, the necessary compressor power has a major influence on the system's overall efficiency. The system efficiency can be improved through the differential pressure operation of an electrolyzer, whereby the hydrogen is electrochemically-compressed on the cathode side. Simulations by our group [8] show that, depending on the current density of the electrolyzer (up to 3 A cm^{-2}) and the storage pressure (max. 750 bar), an electrolyzer operating pressure of up to 20 bar can be beneficial from a system efficiency aspect. However, in order to achieve pressurized operation, circular electrolyzer designs have typically been used by the industry. The circular design can provide a more uniform clamping pressure distribution via bolts and endplates compared to a rectangular design. For instance, 9.6 kW stacks from Fronius International GmbH were operated in a network of 12 modules with a total output power of up to 100 kW at a maximum operating pressure of 163 bar [9]. Similarly, the Giner GS-10 prototype stack from Giner Electrochemical Systems LLC with a maximum production rate of 5.6 kW [10–12] and GenHy©1000 (developed for the GenHyPEM project) with an operating pressure of up to 50 bar and a hydrogen production rate of 1 $Nm^3\ h^{-1}$ were also connected in series to achieve the desired outputs [13,14]. Experimental short stacks with outputs of 1 kW, an operating pressure of up to 100 bar [15], and a hydrogen production rate of up to 2.5 L/min [16] were also implemented as a circular design. As an example for a rectangular design, three electrolyzers of the type SILYZER 200 from Siemens AG with a peak power of 6 MW_{el} and hydrogen output of 1006 $Nm^3\ h^{-1}$ were operated at the "Energiepark Mainz" facility [6]. In order to be able to attain dynamic high-pressure applications with constant cell compression for a rectangular cell design, Wirkert et al. [17] inserted an electrolyzer stack into a surrounded pressure vessel. The experimental short stacks comprise 10 to 12 cells [10–14,16].

The main disadvantage of circular stack designs is the loss of material during the production of the individual cell components (e.g. the membrane electrode assembly (MEA)) [18] and the associated higher production costs. Circular flow fields must also be optimized with respect to uniform heat, mass and current density distribution for proper and durable cell operation [19].

On the anode side (oxygen generation), porous transport layers (PTLs) made of titanium are typically used to ensure water transport to the electrode and electric contact with the flow field and electrodes. Liu et al. [20] have shown that coating the PTL with iridium or platinum is a crucial strategy to allow the PTL's long-term stability. In addition, the coating of the PTL material leads to an optimization of the contact resistance and therefore to a reduced ohmic resistance [20,21].

Furthermore, when designing a next generation of PEM stacks, one must realize that thinner membranes can significantly increase an electrolyzers' hydrogen production capacity. The influence of membrane thickness on cell performance has been simulated several times in the literature [7,22–24]. Our group [25] was able to achieve current densities of 11 A cm^{-2} at 2 V (corresponding to an electric energy consumption of 53.6 kWh per kg produced hydrogen) in a single cell with an approximately 20 μm thick membrane. However, when reducing the membrane thickness, both H_2 permeation through the membrane and reduced membrane robustness to mechanical stresses during operation must be taken into account, especially in differential pressure operation [7,23]. The risk of permeation can be reduced by implementing recombination catalysts into the MEA [26]. For the here developed stack design, we have therefore considered the increased compression and shear stresses over the membrane [27].

Another important design aspect is the adjustment of PTL compression and associated contact pressure. We [28] have shown that by increasing the compression, the performance of an electrolysis cell can be improved, whereas if the compression of the GDL is too high, hydrogen permeation through the membrane increases. The correlation with contact pressure was also demonstrated by Frensch et al. [29]. Thus, an even contact pressure distribution must be considered in the design of bipolar plates and stacks, as well as when creating innovative stack assembly concepts.

When selecting materials for bipolar plates, different studies on metals with different coating processes can be found in the literature [30,31]. Likewise, different coatings on stainless steel as a base material have been investigated to reaching the long-term stability of bipolar plates in acidic environments [32]. Titanium has been mentioned as a state-of-the-art material for electrolyzer bipolar plates. Additionally, these titanium plates are coated with platinum on the anode side to prevent their passivation or corrosion [18,33]. Therefore, the fabrication costs and the necessary protective layer are largely responsible for the high costs of these bipolar plates [33]. According to Ayers et al. [34], the bipolar plates or separator plates currently account for approximately 48% of the stack costs. In addition to the material costs, the costs of

the manufacturing processes for the different flow fields are decisive here.

We have previously published [18] that machined flow fields have the highest flexibility in terms of design but entail high production costs. Also critical is the extensive time needed during fabrication and large material waste accompanies those production methods. Typical machined flow field structures are pin-type, parallel and serpentine, each of which can be implemented in different designs. Other proposed manufacturing methods are the hydroforming or stamping processes, which have limitations in design parameters and contact areas, and are uncommon for electrolysis [35]. Welding processes are also used to join together the different segments of bipolar plates, which may lead to longer production times. A promising welding procedure to join common electrolysis materials such as titanium is diffusion welding [36]. In this procedure, parts with the same or similar material properties can be joined without deforming their structure. This is especially beneficial for the joining of porous flow fields, such as expanded mesh flow fields. Flow fields consisting of titanium meshes or expanded metal have been described in recent literature, and feature in commercially-available stacks.

Expanded metals feature low production costs and good spatial utilization due to their three-dimensional structures. Via numerical and experimental studies, Lafmejani et al. [37] were able to show that expanded metals guarantee a good mass transfer of water to the MEA and possess good cooling properties, making expanded metal suitable for applications with high current densities.

Further promising experimental studies on expanded metals as flow field plates or porous media have been carried out for both single cell applications [38–41] and stack applications [42,43]. As expanded metals can be described as porous media, the sealing of these flow fields is essential, especially with respect to cross flows. Selamet et al. [41] have already investigated different sealing materials in conjunction with metal meshes. They found that the contact pressure in the area of the flow field was strongly dependent on the sealing materials. With respect to the sealing materials used, attention must be paid to the material properties in terms of long-term stability and mechanical properties during operation. The material properties of different sealing materials have been investigated for PEM fuel cells [27,44–48], and the design of both sealing mechanisms and bipolar plates are relevant, especially when operating at high pressures. Ye et al. [49] showed different sealing mechanisms for fuel cell operation. Here, a distinction needs to be made between frame designs that serve as a hard stop for GDL compression, and flat and O-ring seals.

Here we show the development steps to design bipolar plates for a PEM electrolyzer stack in a one-piece approach. Special attention was given to the requirements of the bipolar plates in relation to the state-of-the-art for the cell components. An expanded metal composite was used as the flow field, which provided a great potential for cost reduction of PEM stacks. Another focus was placed on the mechanical behavior of our cell/stack assembly. Our goal was to continue [38] analysis of the influence of contact pressure on cell performance and time-dependent material properties, such as membrane creeping. We consider of particular importance to achieve a homogenous contact pressure distribution to ensure low contact resistances while avoiding pressure peaks, which can easily lead to membrane failures and degradation phenomena. The new bipolar plate concept was intended for a cross-flow configuration. Its advantages include the compact overall bipolar plate setup and the spatial separation of the anode and cathode side manifolds. Some of the design features and the production technology, described here in detail exemplarily for a specific electrolyzer setup, can easily be transferred to other design concepts or other applications (like e.g. fuel cells or redox flow batteries).

2. Experimental

The development of our novel bipolar plate (BPP in the following) focuses on a cost-effective and robust in stack assembly and operation. The objectives, in detail, are as follows:

1 Easy and failure-tolerant stack assembly The number of stack components should be as small as possible. For the stack assembly itself, the BPP should be derived from one piece.
2 Alternative flow field Conventional flow fields comprising a macroscopic channel rib structure have a negative impact on the homogeneity of mechanical compression and flow distribution in the active area [50]. The BPP should be comprised of structures, that support an improved compression distribution.
3 Usage of low cost mass market components Specifically for the flow field regime of the BPP, different types of porous media, such as metallic tissue, metallic fleece, or expanded metal are off-the-shelf and widely available for numerous applications [51,52]. For the optimized functionality of this type of flow field structure, a combination of different types of porous media or of porous media from the same type but with different porosities is advantageous.

Fig. 1 displays an exploded illustration of our novel concept for the BPP unit. It consists of a total of ten single elements (three expanded metal layers per sandwich) combined into one piece (which we will call the BPP in the following) by diffusion welding. Further on in this chapter, we describe the joining process in detail. With regard to this, it is advantageous but not necessary that all elements are from the same material. To be on the safe side, we select Ti as the sole basic material for the first set of BPP prototypes, as it exhibits good corrosion stability in electrolysis mode, also on the critical anode side (O_2/H_20 environment, temperature up to 80 °C and electric potential above 1.5 V) [32].

At the center of the BPP, a massive Ti plate separates the anode and cathode compartments of two neighboring cells. In order to avoid gas crossover, the plate must be gas-tight for hydrogen and oxygen. Additional elements of the BPP include frames and expanded metal sandwiches positioned on each side of the center plate. The frame inlay sandwich on the anode side also comprises a Ti fleece element.

Fig. 2 illustrates the technical realization of fluid distribution and collection at the cell level. It is important to mention,

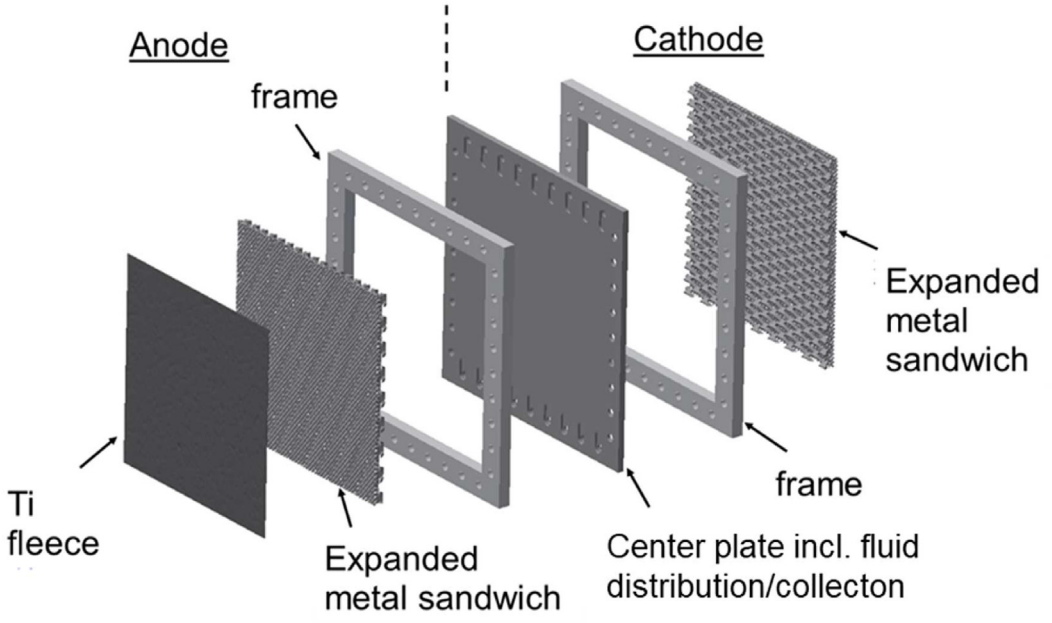

Fig. 1 – Exploded view of the novel bipolar plate unit. All shown elements will be combined to one piece by diffusion welding.

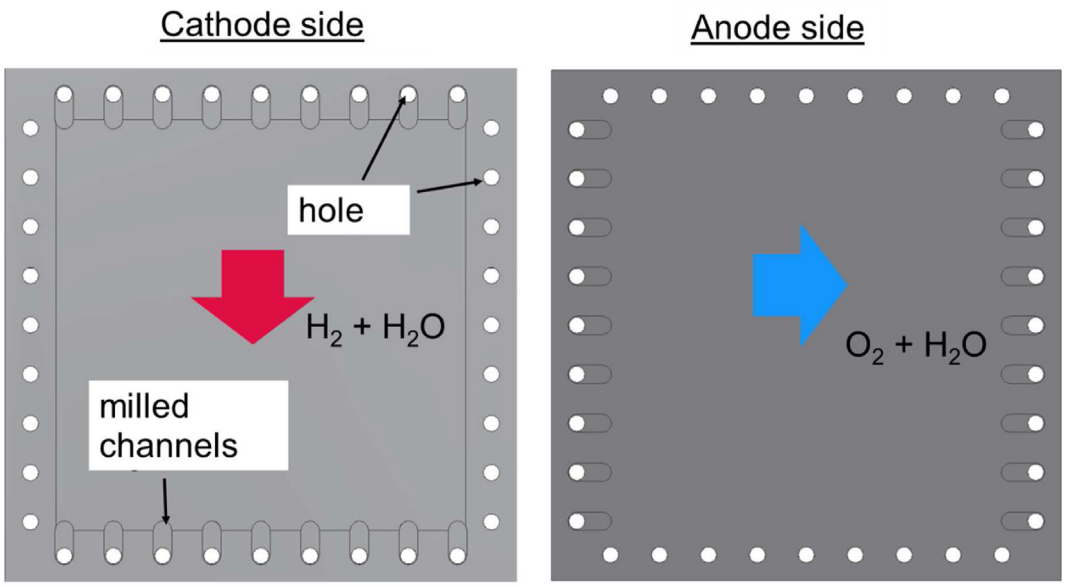

Fig. 2 – Media distribution/collection and main directions of the 2-phase flows on the cathode and anode sides.

that for this BPP concept we assume continuous water circulation on anode and cathode side of the electrolyzer system. Electrochemically water is only consumed at the anode side, but for heating and cooling purposes water loops at high surplus are envisaged for both sides. The BPP (here only the center plate) consists of a row of holes along each rim. Each row of holes interconnects with one of the manifolds of the stacks' fluid distributor/collector. The left sketch in Fig. 2 shows the main flow direction on the cathode side of the plate, when the water inlet is situated at the upper row of holes and the hydrogen/water outlet at the lower one. The water inlet and two-phase flow outlet is possible, because the upper and lower rows of holes are connected to the active cell via milled channels. The symmetrical frame overlaps only a portion of the channels. The right sketch displays the analogous main flow direction on the anode side, which in this example is from left to right. This results overall in a cross-flow configuration for the anode side relative to the cathode side flows.

The sketch in Fig. 3 shows an example of the water inlet entering into the cathode compartment of one cell in greater detail. Coming from one of the stack-level water distribution manifolds, a fraction of the total water flow rate (ideally identical for all the manifolds and for every cell) enters the

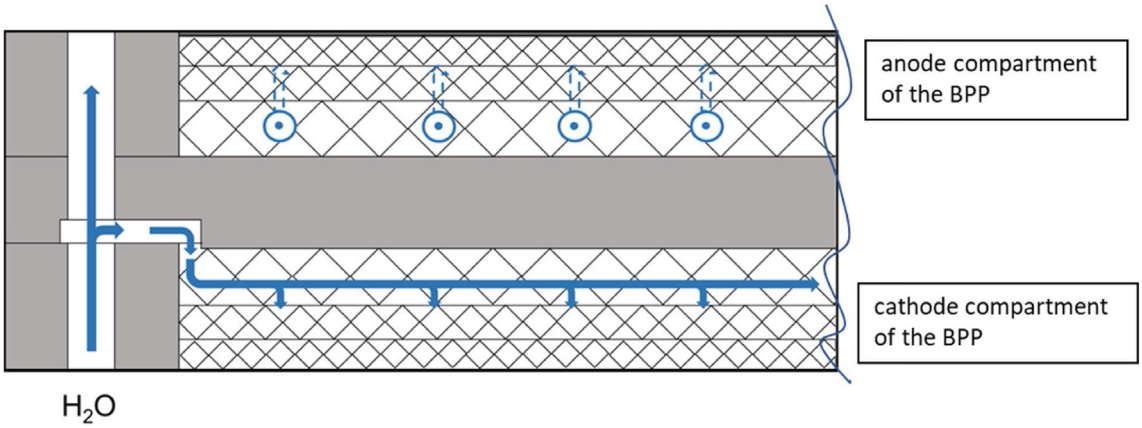

Fig. 3 – Water distribution manifold, water inlet on the cellular level and distribution through the expanded mesh sandwich.

cell's cathode compartment through additional channels in the center plate. These channels are not present on the anode side, and so the rest of the total water flow will separate another fraction into the cathode compartment of the next cell.

The expanded metals used are based on thin metal sheets from Ti Grade 1, machined in such a way that apertures in the form of a diamond occur. The following geometric parameters, also illustrated in Fig. 4, define the shape of the expanded metals:

l: distance between the node points in the direction of the long diagonal

b: distance between the node points in the direction of the short diagonal

c: strand width

s: strand thickness (thickness of the original metal sheet).

a: thickness of expanded metal

For the BPP test design, the expanded metal sandwich consists of three layers with a total thickness of 2.65 mm. Table 1 lists the main geometric parameters of the expanded metal layers.

Compared to a conventional BPP comprising a channel-rib structure, the flow field with expanded metal layers features the following main differences:

- Expanded metals have a regular structure for the fluid flow. It can be considered a porous media. In contrast, conventional flow fields consist of discrete flow channels. Therefore, the fluid flow distribution over the active area is relatively coarse.

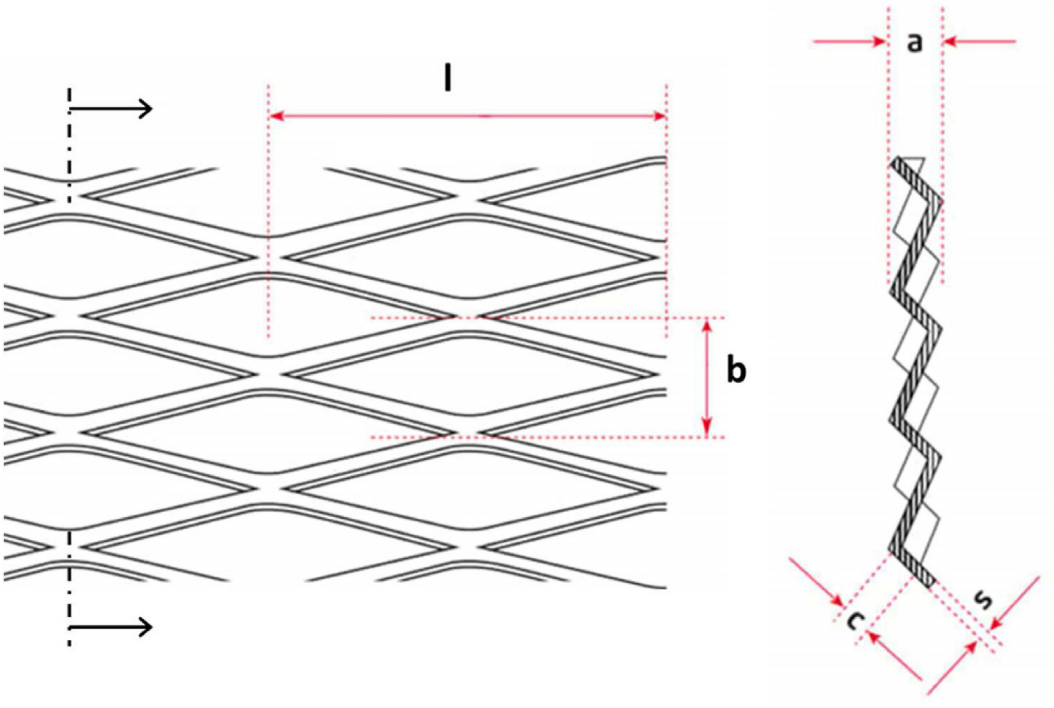

Fig. 4 – Geometric specification of the expanded metals. Left: isometric view, right: cross-section along the strand.

Table 1 – Geometric parameters of the single expanded metals used in the BPP test design sandwich.

Expanded metal No.	l in mm	b in mm	c in mm	s in mm	a in mm
1	2.5	2	0.5	0.5	0.5
2	4	2	0.8	0.5	0.65
3	12	6	1.5	0.8	1.5

- By combining different layers of expanded metal, it is possible to almost continuously refine the flow compartments from the water inlet respectively two-phase flow outlet towards the MEA. With channel-type flow fields, this is not possible.
- In conventional BPPs, the current transmission from the MEA to the BPP only works through the BPP ribs. This means, that about 50% (dependent on the channel/rib structure) of the BPP is electrically unconnected. In addition, the contact area distribution is relatively coarse (analogous to the channels). Expanded metals are connected through the node points of the regular structure.

In addition to the expanded metal sandwiches, the novel one-piece BPP design also includes on the anode side a sheet of Ti fleece. In the cell or stack setup, this serves as the porous transport layer (PTL) to the catalyst layer. For the BPP test design Bekipor® Titanium, 2GDL10-0,35 from NV Bekaert SA (Belgium) with a total thickness of 0.35 mm was used. The material porosity is 68% with a Ti fiber diameter of 20 μm.

Summing up the thicknesses of all components, as shown in Fig. 1, we achieve for our first BPP prototype a cell pitch of 8.7 mm. In this work, the sizing of the single BPP elements is not optimized in terms of electrolyzer power density. A focus is set on production technology and proof of concept.

Once titanium had been selected as the component material, the need for a joining technique appropriate to it and other components became clear. The joining strategy must consider the material and geometry requirements. ZEA-1 at the Forschungszentrum Jülich, as the engineering partner for this research, was involved in the development of the individual components to determine a suitable joining process. The monopolar and bipolar plates, as well as the frames, which are crisscrossed by channels, must be joined gas-tight between the anode and cathode sides and to the outside. In addition, it is necessary that the expanded metal and Ti fleece be joined with the largest possible contact area to maximize electrical conductivity. The Ti fleece must remain open-pored in order to permit mass transfer between the active cell area and flow field. The electrons to be transferred can reach current density values greater than 3 A cm^{-2} at 80 °C. The requirements rule out a soldering or bonding process, as the open and fine-mesh structures would be closed by means of adhesives or solder. Common fusion welding processes such as laser and electron beam welding or even arc welding, cannot provide a full-surface connection of the components and would cause considerable deformations due to the presence of local melting or stress areas.

For these reasons, diffusion welding was selected as the joining method for the monopolar and bipolar plates. Due to its high affinity for nitrogen and oxygen, titanium must be welded under a vacuum or using a pure inert gas atmosphere. As the diffusion welding process takes place in a vacuum, it is especially suitable for the joining of titanium. In diffusion welding, an external application of force, usually in the form of pressure pads, creates contact between the partners to be joined. Simultaneous heating up to approximately 70% of the liquidus temperature can stimulate mass transfer, thus enabling grain growth across the joining surface. This allows large-area and tight joints to be produced with low component distortion. The associated equipment of the ZEA-1 is shown in Fig. 5.

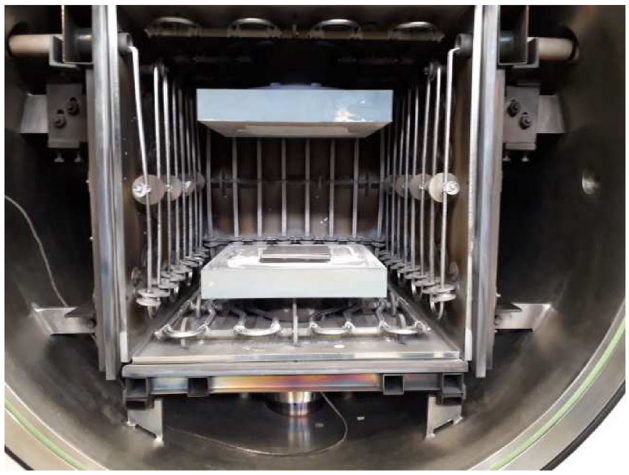

Fig. 5 – Diffusion welding machine of the ZEA-1 with the door open. In addition to the heating elements, the base plate with the bipolar plate to be joined and the ram are visible.

3. Results

In order to demonstrate the suitability of diffusion bonding for the selected Ti Grade 2 plates, multi-level joining tests were initially carried out with the test plates. From our own preliminary investigations, it is known that titanium can be joined by means of diffusion bonding without pre-machining by metal cutting. With a view to efficient and economical process control, five sheet metal frames were stacked on top of each other and joined to form a frame for an initial process value determination (see Fig. 6). The sheet surfaces were degreased with ethanol immediately prior to the furnace process. One area of the sheets was welded with pickling pretreatment and one without it.

The suitability of diffusion welding was demonstrated in principle by means of the helium leakage test and metallographic microstructure analysis. The joining zones not subject to pickling pretreatment exhibited a more uniform diffusion zone without a pronounced pore line (see Fig. 7). The leakage rates of both multi-sheet joints are below $5 \cdot 10^{-9}$ mbar L s^{-1}. Joining was carried out above the transformation temperature of 885 °C applicable to pure titanium. A setting amount per level of approximately 0.1 mm was set by limiting the stroke of the ram. The joining pressure was at about 10 MPa.

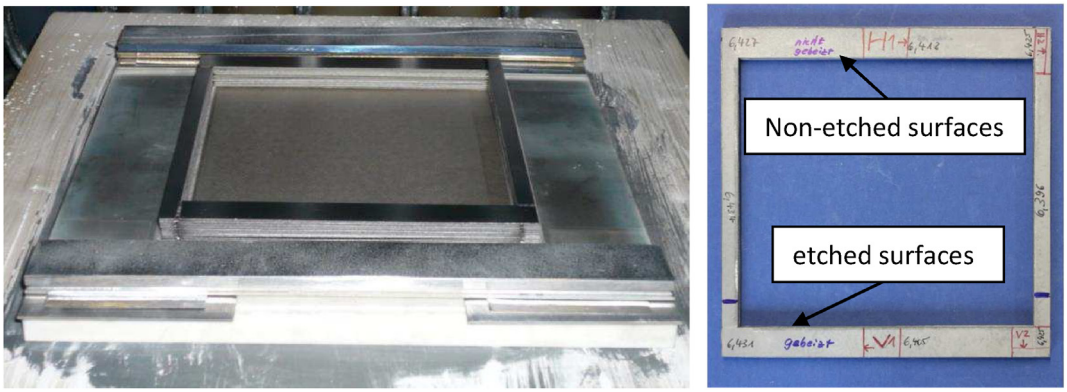

Fig. 6 – Process validation, assembly of five frames before (left) and after (right) diffusion welding.

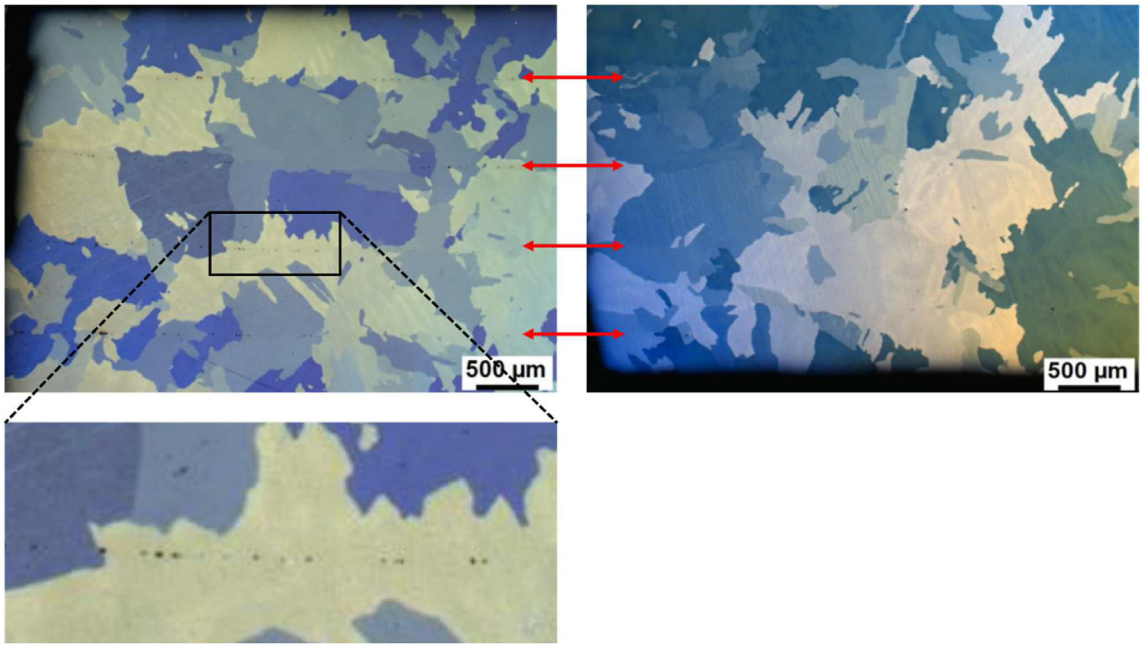

Fig. 7 – Process validation, assembly of five frames, structural analysis after diffusion welding, left: etched surfaces; right: non-etched surfaces; red arrows: joining levels. (For interpretation of the references to colour in this figure legend, the reader is referred to the Web version of this article.)

All bipolar plate prototypes could be joined with the required internal and external tightness. Leakage rates $<10^{-8}$ mbar L s^{-1} were determined by means of a helium leakage test. The expanded metal and Ti fleece were fully bonded. The gap between the expanded metal, Ti fleece, and frame could be reduced to such an extent that the MEA remains undamaged and avoid membrane creeping during operation.

Two further tests were performed to quantify the gain of the single component approach with respect to contact resistance. In the first test, the individual elements of the BPP from Fig. 1 were placed on top of each other and positioned between two gold-plated contact plates (45 mm × 45 mm). A hydraulic press was used to continuously increase the contact pressure on the elements. At the same time, an electric current of about 10 A was passed through the contact plates and the intermediate assembly, and the voltage was measured. The second test was performed identically, only the individual components were replaced by the welded BPP.

At a contact pressure of about 1 MPa, resistances of 153.9 mΩ cm^2 were obtained for the individual elements and 21.4 mΩ cm^2 for the welded BPP. At about 2.5 MPa, 50.3 mΩ cm^2 and 12.8 mΩ cm^2 were determined, respectively. This means that at a target contact pressure on the active cell surface of 2.5 MPa, the resistance of the welded BPP is reduced by about 75% compared to the unwelded version.

In subsequent investigations, scaling up to higher quantities in a joining process will be carried out in collaboration with industrial partners. In this process, several BPP assemblies will be stacked on top of and next to one another in the diffusion welding machine. Important topics here include the development of suitable separating elements between the BPP assemblies and the identification of robust process parameters for diffusion welding. Approaches for the series

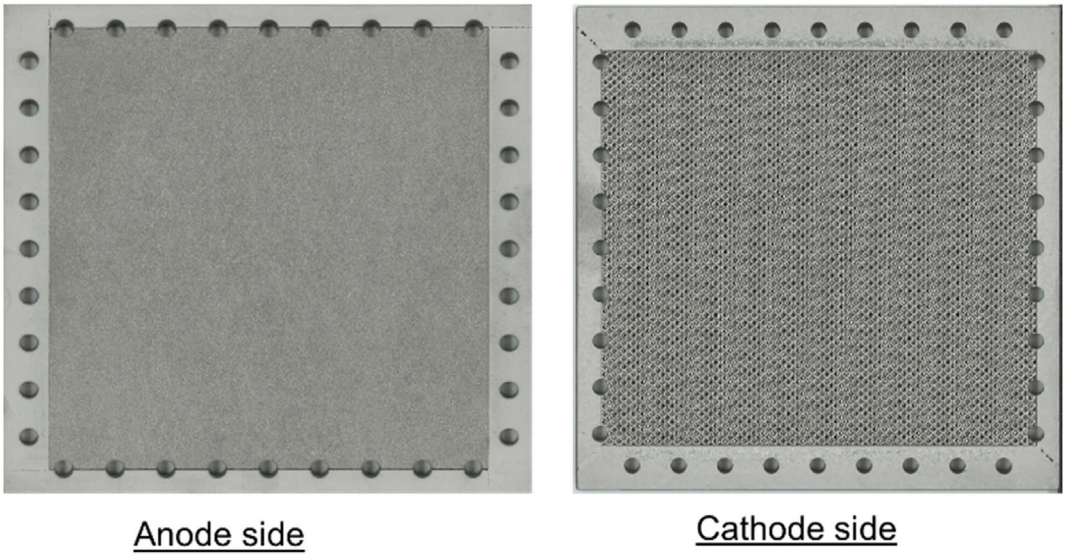

Fig. 8 – Bipolar plate with alternative media distribution and collection, active area of 100 cm^2.

production of larger quantities for MW electrolysis are also being developed at the ZEA-1.

In the following we will demonstrate the proof of concept and production technology with BPPs at 10 cm × 10 cm active cell area. The Ti components of the one-piece BPP are joined by diffusion welding and shown in Fig. 8. The previously described media distribution and collection differs slightly in this case. As Fig. 8 shows, the media excess from the manifolds to the cell level is directly managed by the row of holes and not by the additional channels in the center baffle plate. For the small BPP variant the holes partly encompass the frame and partly the porous materials (expanded metal sandwich on the cathode side and also the Ti fleece on the anode side). In order to separate the anode and cathode sides, the frames consist of two small and two wide sides that face each other. The anode and cathode side frames are turned by 90°.

Fig. 9 shows two cross-sections of the BPP at the transition point between the frame and inner structure. The pictures result from a 3D tomogram, measured by an x-ray computer tomograph (CT), type Xradia 410 Versa from Carl Zeiss AG (Germany).

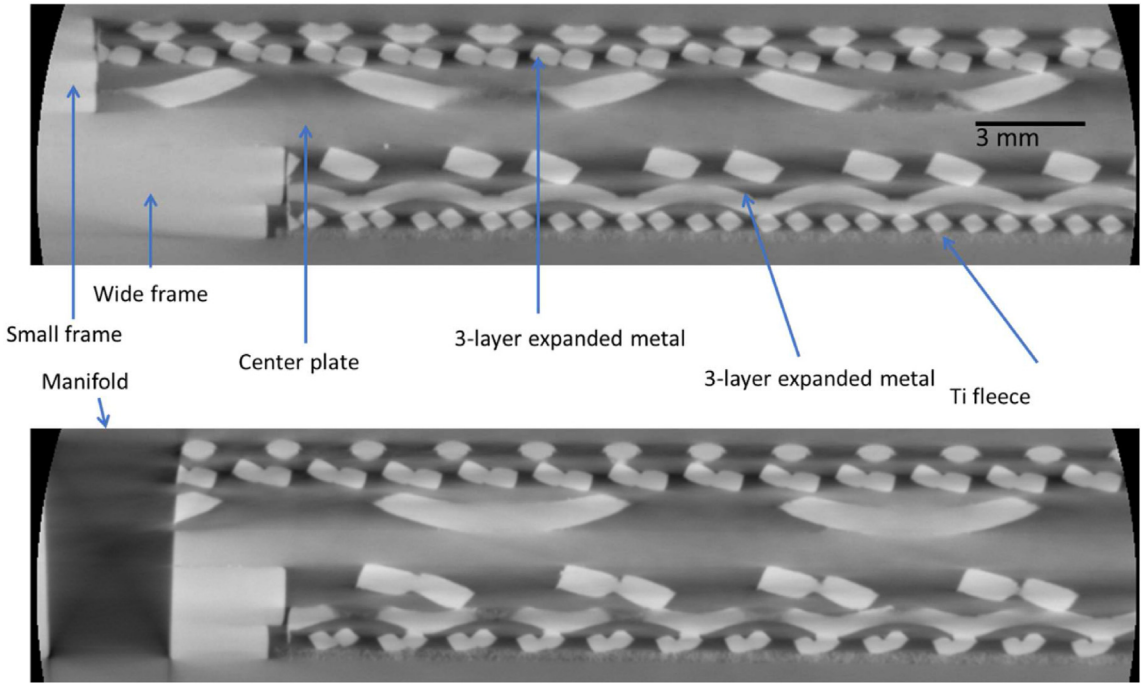

Fig. 9 – Cross-sections of bipolar plate with alternative media distribution and collection and CT data. Upper image: massive frame region; lower picture: frame region at the manifold hole.

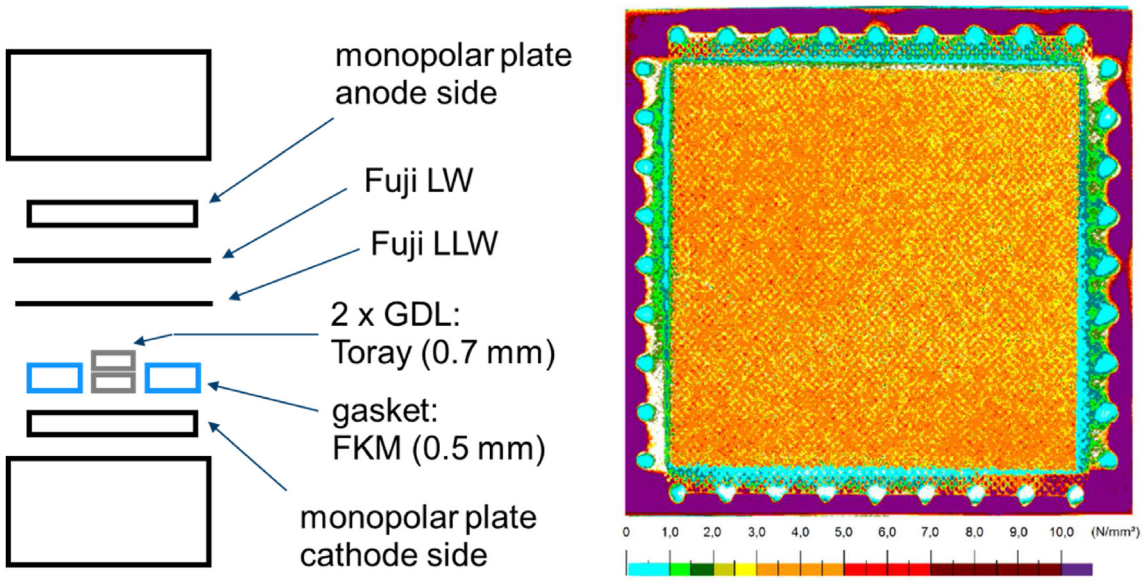

Fig. 10 – Ex-situ test pressure distribution. Left: Schematic sketch of the setup; right: local pressures on the frame and the active area.

The upper image depicts the frame region between the holes. The small and wide frame parts are joined gastight with the center plate. The cross-section through the manifold hole (lower picture) displays the media supply of the cathode compartment (in this case) via the porous edge of the three-layer expanded metal sandwich. The layers are equal for the anode and cathode sides. The porosity of the three layers decreases from the inside to the outside, meaning from the center plate towards the MEA.

Before electrochemical stack testing an ex-situ test was performed to evaluate the homogeneity of the pressure distribution on the active cell area, influenced by the BPP. Fig. 10 displays a scheme of the test setup and results from the test. The anode and cathode side monopolar plates (MPPs) were arranged between two large stamps of a hydraulic press. Starting from the cathode side MPP, a 0.5 mm thick FKM gasket covered the MPP frame and two sheets of Toray paper (total thickness: 0.7 mm) encompass the expanded metal regime. Two sheets of Fujifilm Prescale® enable measurement of the local contact pressure. To cover the full range of pressure distributions on the frame and the active area, the setup comprises Prescale® LLW (0.5–2.5 MPa) Prescale® LW (2.5–10 MPa). Using a scanner and the data analysis software FPD-8010E from Fujifilm, the different red shades from both pressure-sensitive films can be transferred and combined to one new color scale that represents the full pressure range of 0.5–10 MPa. An average pressure of 6 MPa was applied to the setup by the hydraulic press. The holding time was 5 min. The right-hand segment of Fig. 10 shows the pressure distribution in the regions of the active area and outer frame. According to the chosen setup, both monopolar plates influence the pressure distribution.

Three different regimes with significantly different pressure ranges occur. In the active area, the pressure primarily varies between 2.5 and 5 MPa. The overall homogeneity of the pressure distribution is very high. The characteristic pattern of the pressure distribution shows, that the structure of the expanded mesh influences the local pressure on a fine scale (2–2.5 mm). The small pressure peaks at 5 MPa and above are indicators of the sharp edges in the 3D structure (cf. Fig. 4). Even the Ti fleece on the anode side and the carbon paper on the cathode one do not fully homogenize locally. In a real cell or stack setup, this could lead to increased local shear stresses in the membrane. On the other hand, this result indicates that the contact elements for current and heat transfer are well-distributed.

The second regime is the intersection between the active area and frame. Due to our special concept for sealing and media supply for the BPP test design, an overlapping of the stiff frame and porous materials occurs. For the sealing of the cell between the anode and cathode sides, this could be problematic, as the mechanical support is not optimal. This phenomenon results in relatively low pressures of below 1 MPa and up to 2 MPa in the intersection regime. Most critical for eventual leakages are the plate corners, where supply holes for the anode and cathode sides are close to each other.

The third regime is the outer frame area. Here, the contact pressure is largely above 10 MPa, which is necessary to ensure a gas tight setup to the outside.

The test stack consisted of five cells with an active cell area of 100 cm^2. Aside from the BPPs, the main stack components are a fluid distributor/collector for anode and cathode side and current collector plates which are connected to the power supply via gold plated Cu bolts, penetrating central holes in the end plates. The MEA comprises a catalyst-coated membrane (CCM) and porous transport layers (PTLs) on the cathode and anode sides. As mentioned previously, a specialty of this setup is, that the anode-side PTL (Ti fleece) is a fixed element of the one-piece BPP. On the cathode side, two sheets of Toray TGP-H-120 (350 μm each) serve as the PTL and catalyst backing layer. This is a Teflon-treated carbon fiber paper with hydrophobic properties. The in-house-produced CCM is based on

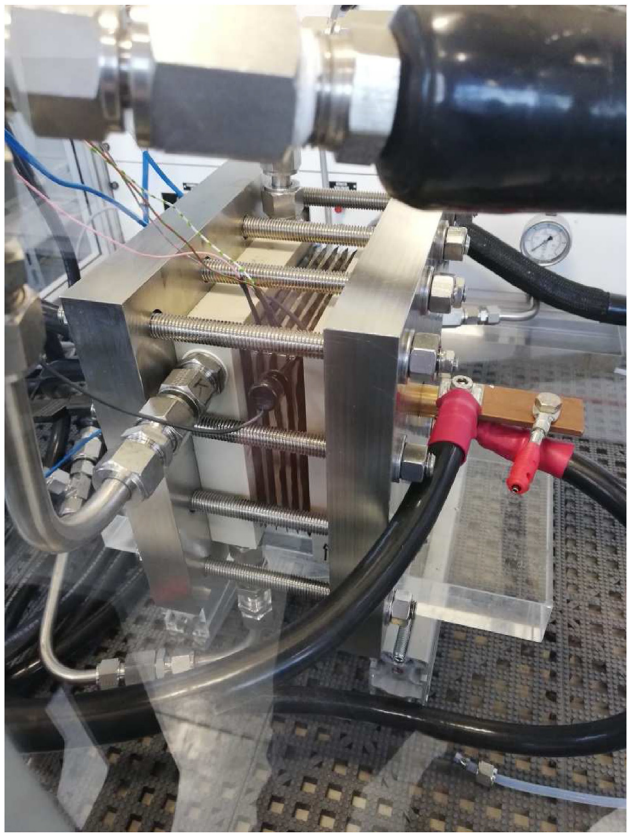

Fig. 11 – Assembled five-cell short stack after test rig integration.

Nafion NR212. Pt/C with 60 wt.-% Pt on ketjen black with a loading of 0.25 mg_{Pt} cm^{-2} is used on the cathode. The anode-side catalyst is IrO_2 from Alpha Aesar with a loading of 1.0 mg_{Ir} cm^{-2}. In order to reduce the risk of the formation of explosive gas mixtures (hydrogen in oxygen on the anode side), the CCM contains a recombination catalyst inside the membrane phase. The manufacture and the effectiveness of the hydrogen reduction on the anode side was shown by our group [26]. Flat gaskets from Viton at 65 shore A and a thickness of 500 μm were used for the stack sealing.

Fig. 11 shows the stack after integration into the test station type ETS G500/G12-290 from Greenlight Innovation Corp. Water cycles on the anode and cathode sides ensure water supply and gas removal. The cycles also utilize circulation pumps and gas separators, as well as heaters and coolers. The test stations' software controls such parameters as temperature, flow rates and stack current respectively voltage. Automated long-term operation is possible, with gas sensors ensuring safety in case of H_2 leakages.

In this paper, we will only report the very first results with the test stack in electrolysis operation. The focus is set on the technological aspects of design and manufacturing. Further operational results with upscaled BPPs will be published later. Fig. 12 displays the initial polarization curve of each single cell in the stack.

During the hold time of 15 min of each step of the polarization curve, the stack current is kept constant (galvanostatic mode). The polarization curve shows averaged voltage values of the last 10 s. Due to the test station restrictions, the maximum drawn current density is at 2.15 A cm^{-2}. For this reason, the test stack was also only operated up to these values. In this range, the stack exhibits an expected behavior. From 0.3 A cm^{-2} to maximum current, mainly ohmic resistances dominate the profile and transport losses are not apparent. This indicates a sufficient media supply and removal, assisted by the porous media of the bipolar plate. The voltage deviation between the five cells increases with increasing current density. Cell No. 3 is slightly (max. 18 mV at the highest current density) worse than the others. Cell No. 3 is located in the middle of the stack. Because of the lack of

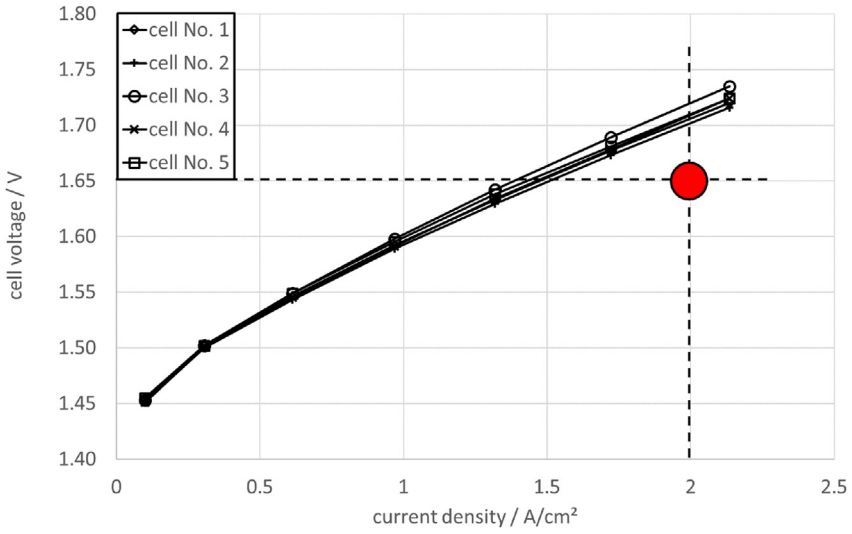

Fig. 12 – Initial polarization curves for each cell of the five-cell short stack. Anode- and cathode-side water loop: 1 L/min; temperature anode/cathode: 80 °C; red dot: target design point, as achieved with a lab cell comprising coatings on the flow fields. (For interpretation of the references to colour in this figure legend, the reader is referred to the Web version of this article.)

stack isolation, one would expect the center cell to have slightly better performance (higher local temperature). This is not the case. Possible reasons for the present situation could be:

- CCM of cell No. 3 performs worse due to production inhomogeneities.
- Inhomogeneities in compression pressure on the active area of cell No. 3 caused by dimensional tolerances.
- Inhomogeneities of water supply or water/gas removal in cell No. 3 caused by dimensional tolerances of the flow channels.

An average voltage of 1.71 V is measured at 2 A cm^{-2}. Thus, the target design point (1.65 V at 2 A cm^{-2}) is not fully achieved. The difference of the 60 mV can mainly be attributed to the lack of coatings for the novel BPPs used (neither for the Ti fleece on the anode side nor for the Ti expanded metal on the cathode side). Ti has a weak tendency to form passivation layers. Contact resistances for the Ti fleece and the anode-side catalyst layer, as well as for the expanded metal and toray paper (cathode side) will increase. The standard test cell from Forschungszentrum Jülich, IEK-14, defining the target design point, comprises Au coating on the anode-side flow field plate and Pt coating on the cathode-side plate.

4. Conclusions

The idea of a one-piece BPP that incorporates standardized elements is a promising approach. Here we have used existing manufacturing technologies, such as the diffusion welding process considered here. A mechanically robust BPP can be produced from simple basic elements. This considerably reduces typical manufacturing efforts and numeral steps during stack assembly. The form-locked joining of the components yields the following additional advantages:

- Safe separation of the anode and cathode compartments of two adjacent cells (transverse tightness).
- Reliable media sealing to the outside.
- Minimal contact resistance in the stacked structure without coatings. In conventional multi-layer configurations of BPP components and PTL corrosion effects lead to increasing contact resistances between the layers. In diffusion welding we add no additional material to the process. The Ti components are material bonded at the contact nodes or areas. In electrolysis mode, the corrosion stability is increased, because there are less interfaces to form passivation layers.
- A quality assurance process for the BPP can be carried out in advance, independently of installation in the stack.

The use of porous structures such as expanded metals lead to a much more homogeneous contact pressure distribution over the active cell area compared to conventional flow field structures (channel/rib configurations). A homogeneous pressure distribution leads to a more uniform current density distribution over the active cell area, as the contact resistance strongly depends on the contact pressure. The first electrolysis operation with a short stack exhibits a performance close to ideal test cells. The flow field of the single test cell considered for this comparison consists of small and short channels in a channel/rib structure. In a scale-up that incorporates the same flow field type, the flow channels would be significantly larger for a comparable pressure drop. Thus, the gradients in contact pressure would be more pronounced, resulting in a less homogeneous current density distribution. For this reason, it is advantageous to use flow fields with porous structures such as expanded metals in stacks with large active cell areas. Nevertheless, additional tests are necessary to quantify the behavior of the BPP at different operation modes, at part or full load, and with static or dynamic profiles. In addition, the scale-up behavior will be evaluated and presented in a subsequent publication.

For the market introduction of the presented One-piece setup, it is necessary to develop a joining technology for cost-effective mass production. Diffusion bonding as a manufacturing process for BPP is currently not ideal for mass production, as it can only be performed discontinuously in a vacuum furnace. In addition to the joining process, up to 12 h are required for evacuation, heating up, and cooling. The development of a batch process in which the vacuum chamber is filled with a maximum number of BPP components to be joined can be a possible solution. Here, the elements must be arranged next to and on top of each other. For stacking, suitable processes and materials for separating the individual BPP assemblies will be identified. Another possibility to speed-up the process is the use of an inert gas atmosphere instead of a vacuum.

Declaration of competing interest

The authors declare that they have no known competing financial interests or personal relationships that could have appeared to influence the work reported in this paper.

Acknowledgements

The results of this work will be incorporated into the LivingLab Energy Campus (LLEC) project. The LLEC is a scientific and technological platform for the development of highly integrated energy supply systems in the fields of heat, electricity, chemical energy storage, and mobility through adaptive and predictive control strategies. It is funded by the Helmholtz Association. The authors would like to express their special thanks to all project and cooperation partners at the LLEC. We would also like to thank Richard Wegner for his technical assistance.

REFERENCES

[1] Zhang Q, Ishihara KN, McLellan BC, Tezuka T. Scenario analysis on future electricity supply and demand in Japan. Energy 2012;38:376–85. https://doi.org/10.1016/j.energy.2011.11.046.

[2] Ghasemian S, Faridzad A, Abbaszadeh P, Taklif A, Ghasemi A, Hafezi R. An overview of global energy scenarios by 2040: identifying the driving forces using cross-impact analysis method. Int J Environ Sci Technol 2020. https://doi.org/10.1007/s13762-020-02738-5.
[3] Zappa W, Junginger M, van den Broek M. Is a 100% renewable European power system feasible by 2050? Appl Energy 2019;233–234:1027–50. https://doi.org/10.1016/j.apenergy.2018.08.109.
[4] Pinsky R, Sabharwall P, Hartvigsen J, O'Brien J. Comparative review of hydrogen production technologies for nuclear hybrid energy systems. Prog Nucl Energy 2020;123:103317. https://doi.org/10.1016/j.pnucene.2020.103317.
[5] Michaelis J, Junker J, Wietschel M. Eine Bewertung der Regelenergievermarktung im Power-to-Gas-Konzept. Z Energiewirtschaft 2013;37:161–75. https://doi.org/10.1007/s12398-013-0113-9.
[6] Kopp M, Coleman D, Stiller C, Scheffer K, Aichinger J, Scheppat B. Energiepark Mainz: technical and economic analysis of the worldwide largest Power-to-Gas plant with PEM electrolysis. Int J Hydrogen Energy 2017;42:13311–20. https://doi.org/10.1016/j.ijhydene.2016.12.145.
[7] Scheepers F, Stähler M, Stähler A, Rauls E, Müller M, Carmo M, et al. Improving the efficiency of PEM electrolyzers through membrane-specific pressure optimization. Energies 2020;13:612.
[8] Tjarks G, Gibelhaus A, Lanzerath F, Müller M, Bardow A, Stolten D. Energetically-optimal PEM electrolyzer pressure in power-to-gas plants. Appl Energy 2018;218:192–8. https://doi.org/10.1016/j.apenergy.2018.02.155.
[9] Sartory M, Wallnöfer-Ogris E, Salman P, Fellinger T, Justl M, Trattner A, et al. Theoretical and experimental analysis of an asymmetric high pressure PEM water electrolyser up to 155 bar. Int J Hydrogen Energy 2017;42:30493–508. https://doi.org/10.1016/j.ijhydene.2017.10.112.
[10] Santarelli M, Medina P, Calì M. Fitting regression model and experimental validation for a high-pressure PEM electrolyzer. Int J Hydrogen Energy 2009;34:2519–30. https://doi.org/10.1016/j.ijhydene.2008.11.036.
[11] Marangio F, Santarelli M, Calì M. Theoretical model and experimental analysis of a high pressure PEM water electrolyser for hydrogen production. Int J Hydrogen Energy 2009;34:1143–58. https://doi.org/10.1016/j.ijhydene.2008.11.083.
[12] Marangio F, Pagani M, Santarelli M, Calì M. Concept of a high pressure PEM electrolyser prototype. Int J Hydrogen Energy 2011;36:7807–15. https://doi.org/10.1016/j.ijhydene.2011.01.091.
[13] Millet P, Ngameni R, Grigoriev SA, Mbemba N, Brisset F, Ranjbari A, et al. PEM water electrolyzers: from electrocatalysis to stack development. Int J Hydrogen Energy 2010;35:5043–52. https://doi.org/10.1016/j.ijhydene.2009.09.015.
[14] Grigoriev SA, Porembskiy VI, Korobtsev SV, Fateev VN, Auprêtre F, Millet P. High-pressure PEM water electrolysis and corresponding safety issues. Int J Hydrogen Energy 2011;36:2721–8. https://doi.org/10.1016/j.ijhydene.2010.03.058.
[15] Farnes J, Bokach D, Hoopen S, Skåtun K, Schautz M, Geneste X, et al. Optimized high temperature PEM fuel cell & high pressure PEM electrolyser for regenerative fuel cell systems in geo telecommunication satellites. Thessaloniki, Greece: 11th European Space Power Conference; 2016.
[16] Selamet ÖF, Becerikli F, Mat MD, Kaplan Y. Development and testing of a highly efficient proton exchange membrane (PEM) electrolyzer stack. Int J Hydrogen Energy 2011;36:11480–7. https://doi.org/10.1016/j.ijhydene.2011.01.129.
[17] Wirkert FJ, Roth J, Jagalski S, Neuhaus P, Rost U, Brodmann M. A modular design approach for PEM electrolyser systems with homogeneous operation conditions and highly efficient heat management. Int J Hydrogen Energy 2020;45:1226–35. https://doi.org/10.1016/j.ijhydene.2019.03.185.
[18] Mergel J, Fritz DL, Carmo M. Stack technology for PEM electrolysis. Hydrogen Science and Engineering : Materials, Processes, Systems and Technology 2016:331–58.
[19] Olesen AC, Frensch SH, Kær SK. Towards uniformly distributed heat, mass and charge: a flow field design study for high pressure and high current density operation of PEM electrolysis cells. Electrochim Acta 2019;293:476–95. https://doi.org/10.1016/j.electacta.2018.10.008.
[20] Liu C, Carmo M, Bender G, Everwand A, Lickert T, Young JL, et al. Performance enhancement of PEM electrolyzers through iridium-coated titanium porous transport layers. Electrochem Commun 2018;97:96–9. https://doi.org/10.1016/j.elecom.2018.10.021.
[21] Liu C, Shviro M, Gago AS, Zaccarine SF, Bender G, Gazdzicki P, et al. Exploring the interface of skin-layered titanium fibers for electrochemical water splitting. Adv Energy Mater 2021;11:2002926. https://doi.org/10.1002/aenm.202002926.
[22] Tijani AS, Rahim AHA. Numerical modeling the effect of operating variables on faraday efficiency in PEM electrolyzer. Procedia Technology 2016;26:419–27. https://doi.org/10.1016/j.protcy.2016.08.054.
[23] Schalenbach M, Carmo M, Fritz DL, Mergel J, Stolten D. Pressurized PEM water electrolysis: efficiency and gas crossover. Int J Hydrogen Energy 2013;38:14921–33. https://doi.org/10.1016/j.ijhydene.2013.09.013.
[24] Müller M, Carmo M, Glüsen A, Hehemann M, Saba S, Zwaygardt W, et al. Water management in membrane electrolysis and options for advanced plants. Int J Hydrogen Energy 2019;44:10147–55. https://doi.org/10.1016/j.ijhydene.2019.02.139.
[25] Stähler M, Stähler A, Scheepers F, Carmo M, Stolten D. A completely slot die coated membrane electrode assembly. Int J Hydrogen Energy 2019;44:7053–8. https://doi.org/10.1016/j.ijhydene.2019.02.016.
[26] Stähler A, Stähler M, Scheepers F, Lehnert W, Carmo M. Scalable implementation of recombination catalyst layers to mitigate gas crossover in PEM water electrolyzers. J Electrochem Soc 2022;169:034522. https://doi.org/10.1149/1945-7111/ac5c9b.
[27] Liang P, Qiu D, Peng L, Yi P, Lai X, Ni J. Structure failure of the sealing in the assembly process for proton exchange membrane fuel cells. Int J Hydrogen Energy 2017;42:10217–27. https://doi.org/10.1016/j.ijhydene.2017.01.026.
[28] Stähler M, Stähler A, Scheepers F, Carmo M, Lehnert W, Stolten D. Impact of porous transport layer compression on hydrogen permeation in PEM water electrolysis. Int J Hydrogen Energy 2020;45:4008–14. https://doi.org/10.1016/j.ijhydene.2019.12.016.
[29] Frensch SH, Olesen AC, Araya SS, Kær SK. Model-supported characterization of a PEM water electrolysis cell for the effect of compression. Electrochim Acta 2018;263:228–36. https://doi.org/10.1016/j.electacta.2018.01.040.
[30] Gago A, Ansar A, Gazdzicki P, Wagner N, Arnold J. Low cost bipolar plates for large scale PEM electrolyzers. 2014.
[31] Lettenmeier P, Wang R, Abouatallah R, Saruhan B, Freitag O, Gazdzicki P, et al. Low-cost and durable bipolar plates for proton exchange membrane electrolyzers. Sci Rep 2017;7:44035. https://doi.org/10.1038/srep44035.
[32] Langemann M, Fritz DL, Müller M, Stolten D. Validation and characterization of suitable materials for bipolar plates in PEM water electrolysis. Int J Hydrogen Energy 2015;40:11385–91. https://doi.org/10.1016/j.ijhydene.2015.04.155.
[33] Carmo M, Fritz DL, Mergel J, Stolten D. A comprehensive review on PEM water electrolysis. Int J Hydrogen Energy

2013;38:4901–34. https://doi.org/10.1016/j.ijhydene.2013.01.151.
[34] Ayers KE, Anderson EB, Capuano C, Carter B, Dalton L, Hanlon G, et al. Research advances towards low cost, high efficiency PEM electrolysis. ECS Trans 2019;33:3–15. https://doi.org/10.1149/1.3484496.
[35] Janßen H, Edelmann A, Mildebrath T, Müller P, Lehnert W, Stolten D. Design and experimental validation of an HT-PEFC stack with metallic BPP. Int J Hydrogen Energy 2018;43:18488–97. https://doi.org/10.1016/j.ijhydene.2018.08.058.
[36] Lee H-S, Yoon J-H, Yi Y-M. Fabrication of titanium parts by massive diffusion bonding. J Mater Process Technol 2008;201:280–4. https://doi.org/10.1016/j.jmatprotec.2007.11.183.
[37] Lafmejani SS, Müller M, Olesen AC, Kær SK. Experimental and numerical study of flow in expanded metal plate for water electrolysis applications. J Power Sources 2018;397:334–42. https://doi.org/10.1016/j.jpowsour.2018.07.032.
[38] Borgardt E, Giesenberg L, Reska M, Müller M, Wippermann K, Langemann M, et al. Impact of clamping pressure and stress relaxation on the performance of different polymer electrolyte membrane water electrolysis cell designs. Int J Hydrogen Energy 2019;44:23556–67. https://doi.org/10.1016/j.ijhydene.2019.07.075.
[39] Fallisch A, Schellhase L, Fresko J, Zechmeister M, Zedda M, Ohlmann J, et al. Investigation on PEM water electrolysis cell design and components for a HyCon solar hydrogen generator. Int J Hydrogen Energy 2017;42:13544–53. https://doi.org/10.1016/j.ijhydene.2017.01.166.
[40] Lickert T, Kiermaier ML, Bromberger K, Ghinaiya J, Metz S, Fallisch A, et al. On the influence of the anodic porous transport layer on PEM electrolysis performance at high current densities. Int J Hydrogen Energy 2020;45:6047–58. https://doi.org/10.1016/j.ijhydene.2019.12.204.
[41] Selamet OF, Ergoktas MS. Effects of bolt torque and contact resistance on the performance of the polymer electrolyte membrane electrolyzers. J Power Sources 2015;281:103–13. https://doi.org/10.1016/j.jpowsour.2015.01.162.
[42] Selamet ÖF, Acar MC, Mat MD, Kaplan Y. Effects of operating parameters on the performance of a high-pressure proton exchange membrane electrolyzer. Int J Energy Res 2013;37:457–67. https://doi.org/10.1002/er.2942.
[43] Müller M, Zwaygardt W, Rauls E, Hehemann M, Haas S, Stolt L, et al. Characteristics of a new polymer electrolyte electrolysis technique with only cathodic media supply coupled to a photovoltaic panel. Energies 2019;12:4150.
[44] Dillard D, Guo S, Ellis M, Lesko J, Dillard J, Sayre J, et al. Seals and sealants in PEM fuel cell environments: material, design, and durability challenges. 2004.
[45] Lin C-W, Chien C-H, Tan J, Chao YJ, Van Zee JW. Chemical degradation of five elastomeric seal materials in a simulated and an accelerated PEM fuel cell environment. J Power Sources 2011;196:1955–66. https://doi.org/10.1016/j.jpowsour.2010.10.012.
[46] Qiu D, Liang P, Peng L, Yi P, Lai X, Ni J. Material behavior of rubber sealing for proton exchange membrane fuel cells. Int J Hydrogen Energy 2020;45:5465–73. https://doi.org/10.1016/j.ijhydene.2019.07.232.
[47] Shen L, Xia L, Han T, Wu H, Guo S. Improvement of hardness and compression set properties of EPDM seals with alternating multilayered structure for PEM fuel cells. Int J Hydrogen Energy 2016;41:23164–72. https://doi.org/10.1016/j.ijhydene.2016.11.006.
[48] Tan J, Chao YJ, Yang M, Lee W-K, Van Zee JW. Chemical and mechanical stability of a Silicone gasket material exposed to PEM fuel cell environment. Int J Hydrogen Energy 2011;36:1846–52. https://doi.org/10.1016/j.ijhydene.2009.12.048.
[49] Ye D-h, Zhan Z-g. A review on the sealing structures of membrane electrode assembly of proton exchange membrane fuel cells. J Power Sources 2013;231:285–92. https://doi.org/10.1016/j.jpowsour.2013.01.009.
[50] Hoppe E, Janßen H, Müller M, Lehnert W. The impact of flow field plate misalignment on the gas diffusion layer intrusion and performance of a high-temperature polymer electrolyte fuel cell. J Power Sources 2021;501:230036. https://doi.org/10.1016/j.jpowsour.2021.230036.
[51] Smith D, Graciano C, Martínez G. Expanded metal: a review of manufacturing, applications and structural performance. Thin-Walled Struct 2021;160:107371. https://doi.org/10.1016/j.tws.2020.107371.
[52] Peukert W. High temperature filtration in the process industry. Filtrat Separ 1998;35:461–4. https://doi.org/10.1016/S0015-1882(98)80015-3.